

# A Single Second Shell Amino Acid Determines Affinity and Kinetics of Linagliptin Binding to Type 4 Dipeptidyl Peptidase and Fibroblast Activation Protein

Gisela Schnapp,<sup>\*[a]</sup> Yvette Hoevels,<sup>[a]</sup> Remko A. Bakker,<sup>[b]</sup> Patrick Schreiner,<sup>[c]</sup> Thomas Klein,<sup>[b]</sup> and Herbert Nar<sup>[a]</sup>

Drugs targeting type 4 dipeptidyl peptidase (DPP-4) are beneficial for glycemic control, whereas fibroblast activation protein alpha (FAP- $\alpha$ ) is a potential target for cancer therapies. Unlike other gliptins, linagliptin displays FAP inhibition. We compared biophysical and structural characteristics of linagliptin binding to DPP-4 and FAP to better understand what differentiates linagliptin from other gliptins. Linagliptin exhibited high binding affinity ( $K_D$ ) and a slow off-rate ( $k_{off}$ ) when dissociating from DPP-4 ( $K_D$  6.6 pM;  $k_{off}$   $5.1 \times 10^{-5} \text{ s}^{-1}$ ), and

weaker inhibitory potency to FAP ( $K_D$  301 nM;  $k_{off} > 1 \text{ s}^{-1}$ ). Co-structures of linagliptin with DPP-4 or FAP were similar except for one second shell amino acid difference: Asp663 (DPP-4) and Ala657 (FAP). pH dependence of enzymatic activities and binding of linagliptin for DPP-4 and FAP are dependent on this single amino acid difference. While linagliptin may not display any anticancer activity at therapeutic doses, our findings may guide future studies for the development of optimized inhibitors.

## Introduction

Human type 4 dipeptidyl peptidase (DPP-4) and fibroblast activation protein alpha (FAP- $\alpha$ ) are representatives of the S9B prolyl oligopeptidase subfamily of the SC clan proteases, which typically comprise serine proteases that cleave peptide substrates after a proline residue. This protease subfamily includes DPP-4, -6, -8, and -9; prolyl oligopeptidase; acylpeptide hydrolase; and prolyl carboxypeptidase, and has been implicated in the pathophysiology of several diseases including type 2 diabetes mellitus (T2DM) and certain forms of cancer.<sup>[1–3]</sup>

Type 4 dipeptidyl peptidase is expressed ubiquitously and is an important therapeutic target for T2DM because it cleaves and inactivates insulinotropic peptides such as glucagon-like peptide 1 (GLP-1) and glucose-dependent insulinotropic pep-

ptide (GIP).<sup>[4]</sup> Inhibition of DPP-4 limits GLP-1 and GIP metabolic breakdown, leading to improved glycemic control in patients with T2DM. Currently there are eight commercially available DPP-4 inhibitors for the treatment of T2DM.<sup>[5,6]</sup> The proteolytic activity of DPP-4 is specific for N-terminal Xaa-Pro sequences, providing unique substrate specificity.<sup>[7]</sup>

Fibroblast activation protein possesses DPP-4-like exopeptidase activity, and in contrast to DPP-4, also exhibits endopeptidase, gelatinase and collagenase activities.<sup>[8]</sup> Also in contrast to DPP-4, FAP tends to be expressed under specific pathophysiological conditions such as during wound healing, fibrosis, and carcinogenesis. The highly increased expression and proteolytic FAP activity in tumor stroma of epithelial cancers<sup>[2]</sup> relative to non-cancerous tissues<sup>[9–11]</sup> suggests that FAP is a potentially attractive target for new cancer therapies. Fibroblast activation protein can degrade FGF21, an endocrine factor secreted by the liver.<sup>[12]</sup> Inhibition of FAP may thus extend the life of FGF21 and offer additional benefits in certain disorders through its role as a key regulator in metabolic homeostasis.<sup>[13]</sup>

Both DPP-4 and FAP are type II transmembrane proteases and they share 84% amino acid sequence homology (51% identity). They also both feature a short cytoplasmic tail at the N terminus, a transmembrane domain, a  $\beta$ -propeller domain and a C terminal  $\alpha\beta$  hydrolase domain that contains the substrate-binding site, including the catalytic triad consisting of Ser630/624 Asp708/702 His740/734 (DPP-4/FAP amino acid sequence numbering). Crystal structures of DPP-4 and FAP show the arrangement of the 170 kDa functional homodimers and the relative position of the N-terminal and catalytic C terminal domains (Supporting Information Figure S1).<sup>[7,14,15]</sup> The  $\beta$  propeller domain prevents access of large substrates to the active site and positions those amino acids important for substrate recognition in the vicinity of the catalytic machinery.

[a] Dr. G. Schnapp, Y. Hoevels, Dr. H. Nar  
Department of Medicinal Chemistry  
Boehringer Ingelheim Pharma GmbH & Co. KG  
Birkendorferstr. 65  
88397 Biberach (Germany)  
E-mail: gisela.schnapp@boehringer-ingelheim.com

[b] Dr. R. A. Bakker, Dr. T. Klein  
Department of Cardiometabolic Research  
Boehringer Ingelheim Pharma GmbH & Co. KG  
Birkendorferstr. 65  
88397 Biberach (Germany)

[c] Dr. P. Schreiner  
Proteros Biostructures  
Bunsenstr. 7a  
82152 Martinsried (Germany)

Supporting information for this article is available on the WWW under <https://doi.org/10.1002/cmdc.202000591>

© 2020 The Authors. ChemMedChem published by Wiley-VCH GmbH. This is an open access article under the terms of the Creative Commons Attribution Non-Commercial NoDerivs License, which permits use and distribution in any medium, provided the original work is properly cited, the use is non-commercial and no modifications or adaptations are made.

In addition to catalytic residues, other amino acids lining the active site serve key roles in substrate recognition. The hydrophobic S1 pocket of DPP-4, formed by Val656, Tyr631, Tyr662, Trp659, Tyr666, and Val711, determines the specificity for proline as the substrate P1 residue.<sup>[14]</sup> Most importantly, the tandem of Glu205/Glu206 residues in DPP-4 forms a negatively charged hot spot that functions as a recognition site for the amino terminus of peptide substrates, anchoring them in such a way to permit only dipeptide cleavage.

Unlike other gliptins, linagliptin, with a half maximal inhibitory concentration ( $IC_{50}$ ) for DPP-4 of 1 nM, also inhibits human FAP ( $IC_{50}$  89 nM).<sup>[16,17]</sup> Better understanding the features that characterize linagliptin binding to both DPP-4 and FAP could lead to the development of optimized FAP inhibitors or biselective DPP-4/FAP inhibitors that offer utility in a greater range of metabolic disorders.

## Results and Discussion

### Analysis of linagliptin binding kinetics to type 4 dipeptidyl peptidase and fibroblast activation protein

A series of surface plasmon resonance (SPR) experiments were conducted with immobilized DPP-4 or FAP to study the interaction of linagliptin with DPP-4/FAP. As linagliptin binds tightly to DPP-4 we used single cycle kinetic experiments to determine its off-rate.<sup>[18]</sup> The dissociation of linagliptin from human recombinant DPP-4 was slow ( $k_{off}$   $5.1 \times 10^{-5} s^{-1}$ ) (Figure 1A and Table 1).

In contrast, linagliptin dissociated rapidly from human recombinant FAP and exhibited a transient binding at physiologic pH (pH 7.3). Thus, it was not possible to quantify off-rates (Figure 1B). The  $k_{off}$  of linagliptin from FAP at pH 9.0 was markedly slower than at pH 7.3 (Figure 1C). Assuming off-rates greater than  $1 s^{-1}$ , linagliptin dissociated more than 20,000 times faster from FAP than from DPP-4 at physiologic pH.

### pH dependence and binding kinetics of fibroblast activation protein inhibition by linagliptin

Fibroblast activation protein exhibited pH-dependent DPP enzymatic activity (Supporting Information Figure S2A), in line with previous observations.<sup>[19]</sup> Activity peaked at pH 8.5, decreasing markedly as pH fell to approximately 7.5. Enzyme activity was minimal below pH 6. We performed peptidase activity assays for FAP across a range of different pH values to determine its inhibition by linagliptin. Linagliptin inhibited DPP-4 enzymatic activity of FAP in a pH-dependent fashion. As shown in Supporting Information Table S1, the inhibitory potency (as measured by the half maximal inhibitory concentration [ $IC_{50}$ ]) of linagliptin to FAP and DPP-4 increased markedly with rising pH. The  $IC_{50}$  values ranged from 2075 nM at pH 6.0 to 17.1 nM at pH 9.0.

Data from surface plasmon resonance binding studies also reflected an increase in inhibitory potency of linagliptin to FAP

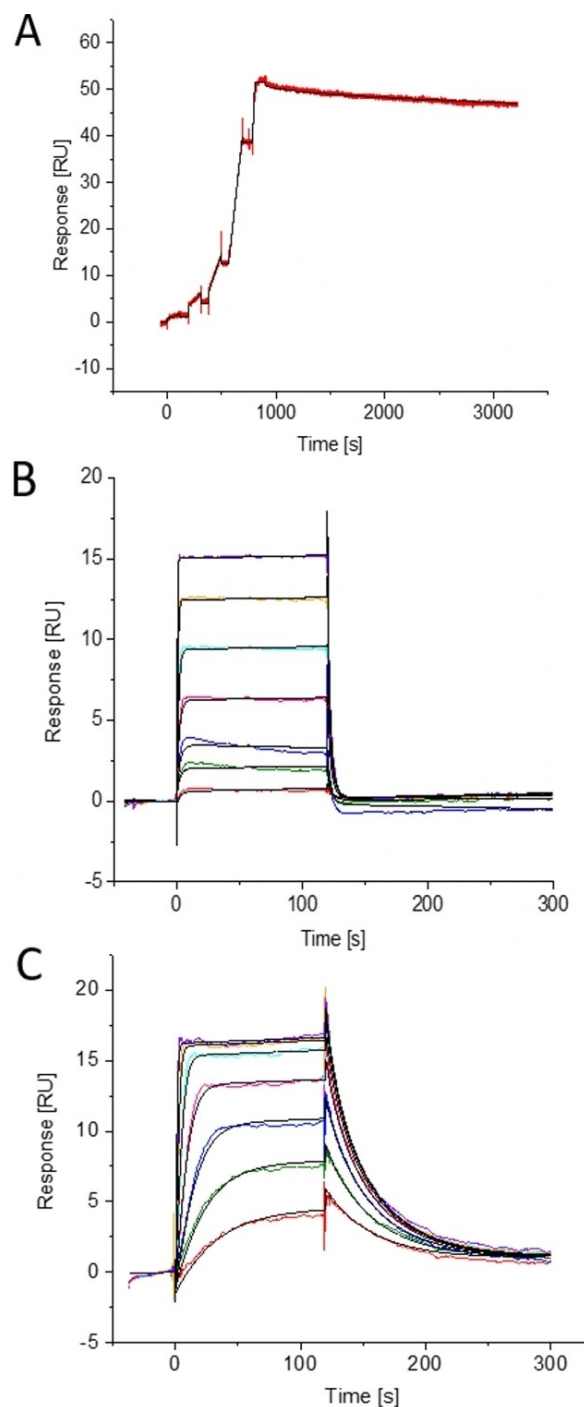


**Figure 1.** Surface plasma resonance (SPR) binding studies to determine the kinetics of linagliptin binding to immobilized (A) DPP-4 at pH 7.3, (B) FAP at pH 7.3, and (C) FAP at pH 9.0. The colored lines represent experimental data and the black lines represent the fitted curves. The sensorgrams show representative SPR experiments (single-cycle kinetic for DPP-4 and multicycle kinetic for FAP). DPP-4: type 4 dipeptidyl peptidase; FAP: fibroblast activation protein; RU: responsive unit.

with rising pH. The affinity dissociation constant ( $K_D$ ) decreased from 6510 nM at pH 6.0 to 15.8 nM at pH 9.0, demonstrating an increased affinity of linagliptin to FAP across this pH range (Supporting Information Table S2). As the  $K_D$  of linagliptin for

**Table 1.** Enzyme inhibition and binding affinity/kinetics data for linagliptin and type 4 dipeptidyl peptidase, fibroblast activation protein, type 4 dipeptidyl peptidase D663A, and fibroblast activation protein A657D at pH 7.3 (surface plasmon resonance data) and 7.5 (IC<sub>50</sub>).

Protein	IC <sub>50</sub> [nM]	K <sub>D</sub> [nM]	k <sub>off</sub> [s <sup>-1</sup> ]	k <sub>on</sub> [M <sup>-1</sup> s <sup>-1</sup> ]
DPP-4	1.4 ± 1.1	0.0066 ± 0.00034	(5.1 ± 1.4) × 10 <sup>-5</sup>	(7.6 ± 1.8) × 10 <sup>6</sup>
DPP-4 (D663A)	1.6 ± 0.7	1.6 ± 0.1	(7.0 ± 0.7) × 10 <sup>-3</sup>	(4.5 ± 0.6) × 10 <sup>6</sup>
FAP	89.9 ± 15.4	301.2 ± 103.3	n.d.	n.d.
FAP (A657D)	1.1 ± 0.7	1.1 ± 0.6	(2.1 ± 1.1) × 10 <sup>-3</sup>	(2.4 ± 1.3) × 10 <sup>6</sup>

DPP-4 = type 4 dipeptidyl peptidase; FAP = fibroblast activation protein; IC<sub>50</sub> = half maximal inhibitory concentration; K<sub>D</sub> = affinity dissociation constant; k<sub>off</sub> = dissociation constant; k<sub>on</sub> = association constant; n.d. = not determined.

Note: The kinetic and enzyme inhibition data were mean values from at least three independent measurements with calculated standard deviation. Kinetic parameters for FAP binding were not determined due to transient binding.

FAP was lower at pH 9.0 than in the range of pH 6.0 to pH 8.5, we were able to quantitate the binding kinetics. Compared with the rapid dissociation of linagliptin for FAP at pH 7.3 ( $k_{\text{off}} > 1 \text{ s}^{-1}$ ),  $k_{\text{off}}$  was  $0.094 \text{ s}^{-1}$ , i.e., greater than 10-fold slower, at pH 9.0 (Figure 1C and Supporting Information Table S2).

Comparison of binding and inhibition data showed that there was a correlation between the negative log of the half maximal inhibitory concentration ( $\text{pIC}_{50}$ ) and negative log of the dissociation constant ( $\text{pK}_D$ ) derived from SPR measurements taken at different pH ( $p < 0.0001$ ,  $r^2 = 0.97$ ) (Figure 2).

Exopeptidase activity of DPP-4 did not appear to be pH dependent within the range of pH 5.5 to pH 8.5 (Supporting Information Figure S2B). In contrast to FAP inhibition, the inhibition of DPP-4 by linagliptin was largely pH independent (1.1 nM at pH 6.0 versus 1.9 nM at pH 8.5; Supporting Information Table S1). However, determination of DPP-4 IC<sub>50</sub> values for inhibition by linagliptin could have been limited by the assay wall, which falls within the 1 nM range in the experimental setting. A direct comparison of quantitative binding and activity data for several DPP-4 inhibitors reported in a previous study showed that the calculated binding affinities ( $K_D$ ) from SPR data are generally lower than those calculated using the biochemical assay, and suggests that the assay wall is a plausible

explanation for this observed difference.<sup>[18]</sup> Linagliptin consistently displayed highest affinity and residence time to DPP-4 amongst the other DPP-4 inhibitors assessed irrespective of the assays used.

### Crystal structures of linagliptin type 4 dipeptidyl peptidase and fibroblast activation protein complexes

We analyzed the linagliptin cocrystal structures of DPP-4<sup>[16]</sup> and FAP (Figure 3 and Supporting Information Figure S3) comparing them with the structures of the unbound proteases<sup>[14,15]</sup> in order to rationalize the observed differences in the binding kinetics of linagliptin.

The aminopiperidine substituent at C-8 of the linagliptin xanthine scaffold occupies the DPP-4 S2 subsite. The primary amine forms a network of charge-reinforced hydrogen (H) bonds to the Glu205, Glu206, and Tyr662 amino acid residues that constitute the recognition site for the amino terminus of peptide substrates of DPP-4. The butynyl substituent at N-7 occupies the hydrophobic S1 pocket of the enzyme. The xanthine moiety is positioned such that its uracil moiety lies on top of Tyr547, forming aromatic  $\pi$ -stacking interactions with the phenol moiety of Tyr547. In this way, the side chain of Tyr547 is pushed back from its 'relaxed' position observed in the uncomplexed<sup>[20]</sup> and the peptide substrate-bound forms.<sup>[14,15]</sup> A similar conformational change has been reported for related xanthine-based inhibitors and for inhibitors from other structural classes.<sup>[21,22]</sup> The C-6 carbonyl function of the xanthine scaffold forms a hydrogen bond with the backbone amino group of Tyr631. Finally, the quinazoline substituent at N-1 is placed on a hydrophobic surface patch of the protein, and interacts with Trp629 by  $\pi$ -stacking its phenyl ring with the pyrrole ring of the amino acid side chain (Figure 3A).

We showed that binding of linagliptin to FAP (Figure 3B) was almost identical to that of binding with DPP-4, with the exception of the distal quinazoline substituent, which was turned by 180 degrees about the exocyclic bond in FAP relative to DPP-4. After analyzing a variety of DPP-4 crystal structures in complex with linagliptin analogs previously, we found that both conformers do not differ greatly in terms of their contribution to the free energy of binding; we often observed one conformer or the other, and sometimes both, with similar occupancy (data not shown).<sup>[18]</sup> All polar and hydrophobic interactions formed

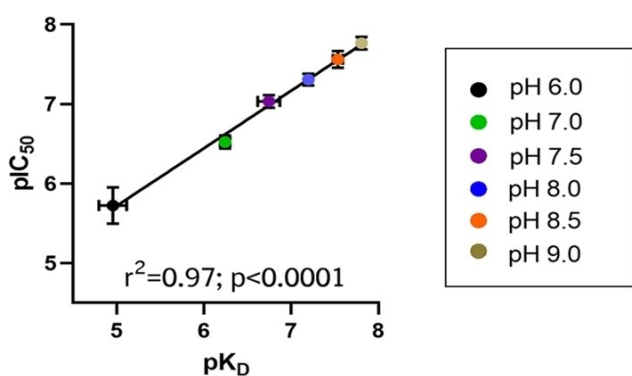


**Figure 2.** Correlation of functional  $\text{pIC}_{50}$  and  $\text{pK}_D$  (determined using surface plasmon resonance; SPR) of linagliptin for fibroblast activation protein at different pH values (indicated by different colors). Three independent experiments were performed for functional IC<sub>50</sub> and four independent measurements for SPR analysis. Data are mean values ± standard deviation, the respective SD bars for each data point are  $\text{pIC}_{50}$  (up and down) and  $\text{pK}_D$  (left and right).  $\text{pIC}_{50}$  = negative log of the half maximal inhibitory concentration IC<sub>50</sub>;  $\text{pK}_D$  = negative log of the dissociation constant  $K_D$ .

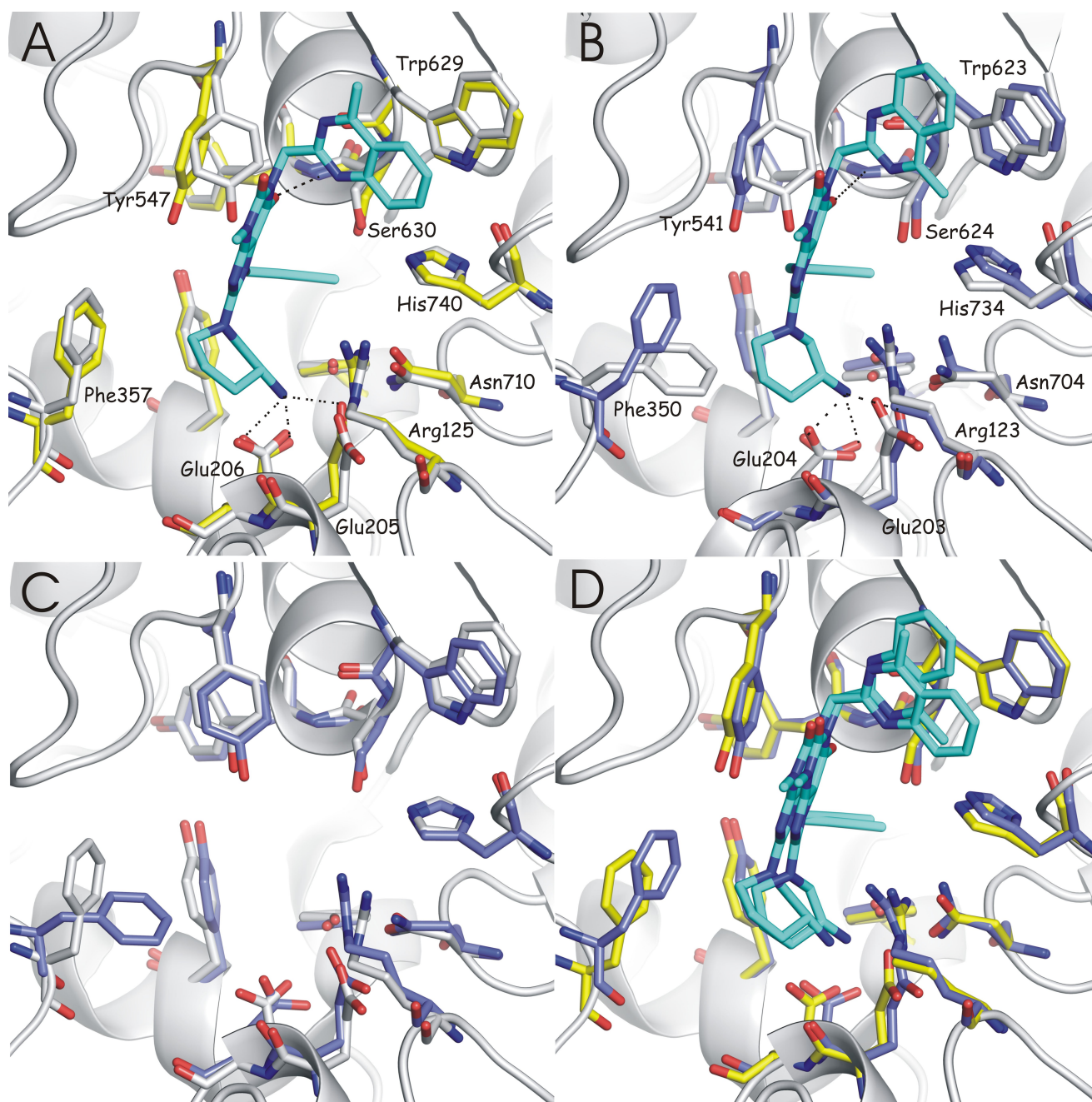


**Figure 3.** Comparison of cocrystal structures of linagliptin bound to DPP-4 and FAP. (A) Cocrystal structure of linagliptin bound to DPP-4 (yellow carbon atoms) superimposed on the ligand-free structure (white carbon atoms). (B) Cocrystal structure of linagliptin bound to FAP (blue carbon atoms) superimposed on the ligand-free structure (white carbon atoms). Comparison of the (C) ligand-free (DPP-4 –, white carbon atoms; FAP –, blue carbon atoms) and (D) linagliptin-bound forms of both proteases (DPP-4 –, yellow carbon atoms; FAP –, blue carbon atoms). DPP-4: type 4 dipeptidyl peptidase; FAP: fibroblast activation protein.

by the ligand were conserved in both complexes, and from this we conclude that conformational change does not have a dominant role in the determination of binding kinetics.<sup>[18]</sup> Comparison of the ligand-bound and unbound forms of FAP has previously revealed a conformational adaptation of the receptor upon ligand binding that involves the residue Tyr541, very similar to the conformational changes described above for DPP-4.<sup>[7]</sup>

A superposition of the unbound (Figure 3C) and bound (Figure 3D) forms of DPP-4 and FAP implies that (i) all the residues lining the linagliptin binding site and contacting the ligand are identical, (ii) the binding mode of linagliptin is identical for the two enzymes with the exception of the quinazoline orientation (*vide infra*), and (iii) the corresponding conformational adaptations of the proteins are strikingly similar, with the only exception being residue Phe357/Phe350, which in

uncomplexed FAP adopts a distinct side chain orientation and is pushed to the position observed in both of the complexes and in uncomplexed DPP-4 upon linagliptin binding.

Given that all residues in the first shell around linagliptin were identical when bound to DPP-4 and FAP, and a similar binding mode of linagliptin was observed, including the conformational adaptations induced by ligand binding, we sought to determine why the linagliptin binding affinity and kinetics differ so markedly between the two enzymes. Studies focusing on the distinct enzyme kinetics and substrate specificity of DPP-4 and FAP<sup>[7,23]</sup> showed a sequence difference in the second shell around the catalytic sites, Asp663 (DPP-4) versus Ala657 (FAP), to be responsible for the behavior observed in this study (Figure 4). We suspected that this difference in amino acids was also responsible for the distinct linagliptin binding phenotypes as well as for the observed pH dependence of enzymatic activity.

#### Type 4 dipeptidyl peptidase D663A and fibroblast activation protein A657D display interchanged linagliptin binding and inhibition behavior

In order to assess the likely role of the single amino acid difference between DPP-4 and FAP in determining distinct linagliptin binding kinetics, we studied binding of linagliptin to the corresponding exchange mutants DPP-4 D663A and FAP A657D (Figure 5). It was suspected that the single amino acid differences between DPP-4 (Asp663) and FAP (Ala657) were responsible for the distinct binding kinetics previously demonstrated.

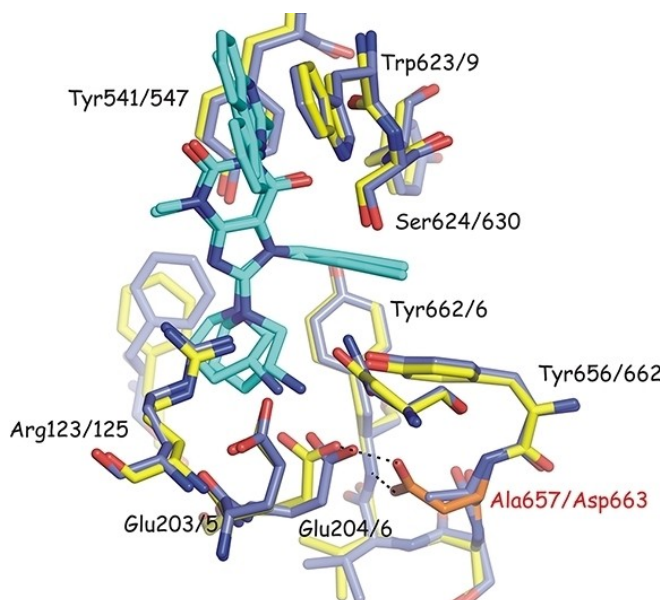


**Figure 4.** Cocrystal structure of linagliptin bound to DPP-4 (yellow carbons) and FAP (blue carbons). A key structural feature, the Asp663 (DPP-4, orange carbons) – Ala657 (FAP) exchange, is responsible for differences in substrate specificity and enzyme activity.<sup>[7,23]</sup> DPP 4: type 4 dipeptidyl peptidase; FAP: fibroblast activation protein.

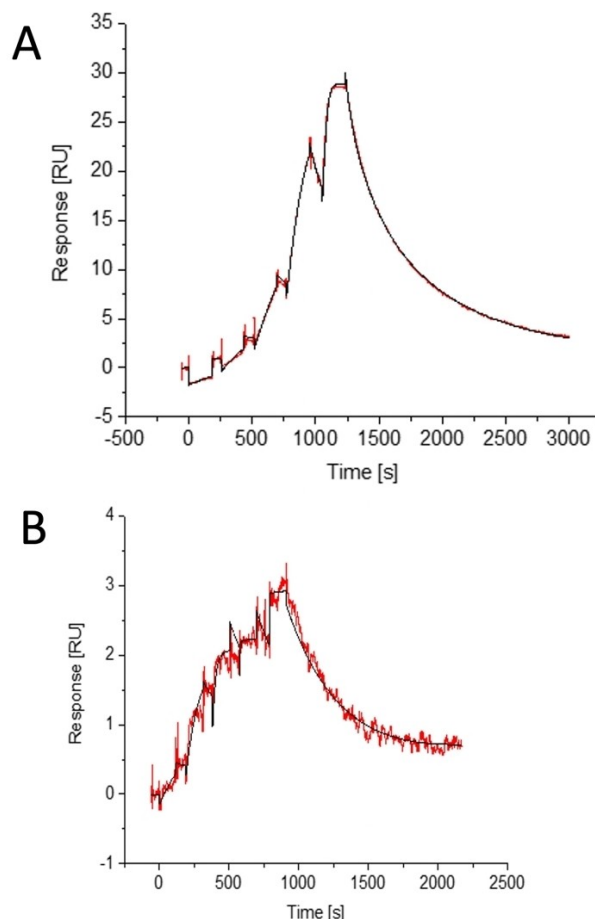


**Figure 5.** Binding kinetics of linagliptin to (A) DPP-4 D663A and (B) FAP A657D mutants studied with SPR. The sensorgrams show representative examples of single-cycle kinetic experiments, in which the red lines represent experimental data and the black lines represent the fitted curves. Immobilization levels were low for the FAP mutant, explaining the relatively low response levels. DPP-4: type 4 dipeptidyl peptidase; FAP: fibroblast activation protein; RU: response unit.

As expected, in contrast to their wild-type counterparts, the binding affinity and kinetics of linagliptin to the exchange mutants DPP-4 D663A and FAP A657D were reversed.

The 'on' rate of linagliptin to DPP-4 is very fast and close to the diffusion limit ( $7.6 \times 10^6 \text{ M}^{-1} \text{ s}^{-1}$ ), and likely to be driven by a rapid electrostatic interaction.<sup>[18]</sup> Electrostatic interactions between a charged drug and a reversely charged protein positively impact association rates.<sup>[24]</sup> The localized positive charge on linagliptin attracts the negatively charged surface patch at the Glu205/Glu206 dyad in the DPP-4 active site, resulting in a strong electrostatic interaction and a fast on-rate. Mutation of Asp663 to Ala in DPP-4 led to a slower on-rate, one that was consistent with a reduced electronegative surface potential of the mutant. Relative to wild-type DPP-4, the binding affinity of the DPP-4 D663A mutant to linagliptin was 242-fold lower with a 137-fold faster off-rate (Figure 5A and Table 1). In contrast, the binding affinity of the FAP A657D mutant to linagliptin relative to wild-type FAP was 273-fold higher and had a slow off-rate with a >400-fold prolonged

residence time (Figure 5B and Table 1). The affinities and binding kinetics of linagliptin to FAP A657D and DPP-4 D663A mutants were consistent with inhibition constants. The  $IC_{50}$  of linagliptin against FAP A657D ( $IC_{50} = 1.1 \text{ nM} \pm 0.7$ ) was markedly reduced compared with wild-type FAP ( $89.9 \text{ nM} \pm 15.4$ ), and was in fact very similar to the  $IC_{50}$  of wild-type DPP-4 ( $1.4 \pm 1.1$ ) (Table 1). As observed above, due to the assay wall of approximately 1 nM setting the  $IC_{50}$  lower limit, further quantitative interpretation of the  $IC_{50}$  data was not possible.

#### pH profile of enzyme activity of mutant proteins

We determined the pH dependence of the enzyme activity of the mutant proteins, and compared the values we obtained with the wild-type protein profiles (Figure 6). As expected from the interchanged linagliptin binding and inhibition behavior demonstrated in the exchange mutants, we observed a similar change in both endo- and exopeptidase activities. Type 4 dipeptidyl peptidase D663A showed high exopeptidase activity

at high pH, which dropped sharply as pH decreased and was inactive below pH 5.5 (Figure 6B). In contrast to wild-type DPP-4 which had no detectable endopeptidase activity between pH 6 and pH 9, the mutant protein had weak endopeptidase activity that demonstrated a bell-shaped profile, peaking at pH 7.5 (Figure 6D). The FAP A657D mutant did not exhibit the pH dependence of exopeptidase activity observed in wild-type FAP and demonstrated high activity in the pH range of 6 to 9 (Figure 6A). This mutant displayed little activity against endo-substrates (Figure 6C).

Collectively, these data imply that the Asp663 and Ala657 residues in DPP-4 and FAP, respectively, were the major determinants of enzymatic activity and ligand binding characteristics, which was consistent with observations in other studies.<sup>[14,23]</sup>

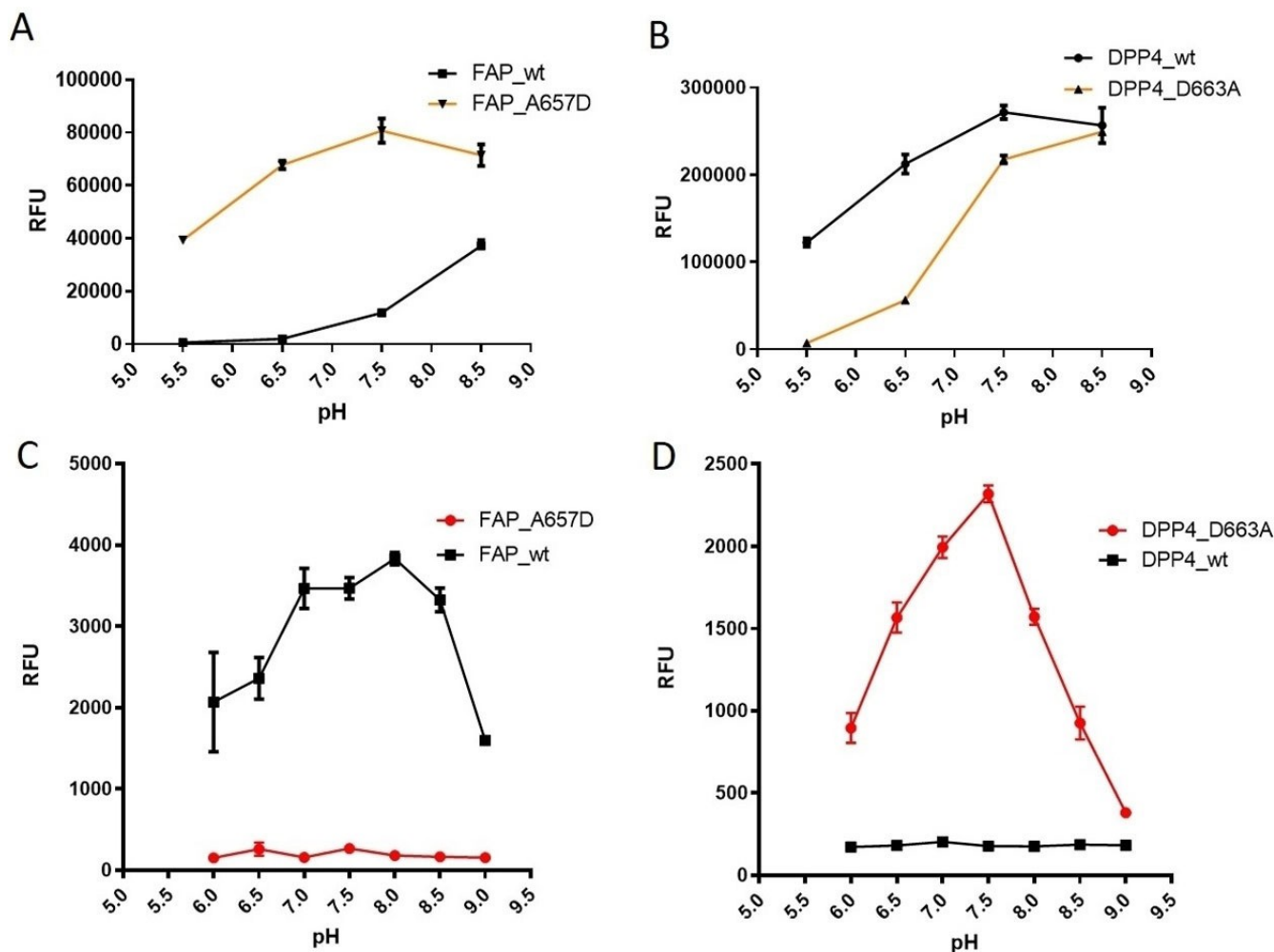


**Figure 6.** The pH-dependent exopeptidase (A and B) and endopeptidase (C and D) activity of FAP and the FAP A657D mutant (A and C) and DPP-4 and the DPP-4 D663A mutant (B and D). Activity of wild-type enzymes is indicated in black, and activity of mutated enzymes is indicated in red or orange. DPP-4: type 4 dipeptidyl peptidase; FAP: fibroblast activation protein; RFU: relative fluorescence unit; wt: wild-type.

### The Asp663/Ala657 sequence variation results in both structural and electrostatic differences between type 4 dipeptidyl peptidase and fibroblast activation protein

Visual inspection of the cocrystal structure of linagliptin bound to DPP-4 and FAP (Figure 4) showed that the side chains of the Ala657/Asp663 residues lie below the phenol ring of residues Tyr656/Tyr662, which forms the lower part of the S1 pocket. In DPP-4, Asp663 is completely shielded from bulk water. It forms a network of close contacts via its carboxylate oxygens. One carboxylate oxygen is within hydrogen-bonding distance of the backbone amino group of Tyr666, thereby being available to serve as a hydrogen-bond acceptor. Quite unusually, the other carboxylate oxygen falls within hydrogen-bonding distance of the carboxylate group of Glu206. Given the hydrogen-bonding pattern, it must be assumed that this side chain is protonated at physiological pH which facilitates a hydrogen-bond donation to Glu206. A structural consequence of the presence of Asp663 would be the rigidification of the Glu206 side chain, orientating the preferred carboxylate hydrogen-bonding lone pairs toward the active site pocket and towards interacting ligands.

In FAP, the Ala657 methyl side chain is less sterically demanding and is not available for any hydrogen bond involvement. The neighboring Glu204 is thus conformationally less strained and more adaptive to requirements of substrate binding. Analysis of the contributors to surface electrostatics (Figure 7) at the Glu dyads suggests that in DPP-4 the hydrogen bonding of protonated Asp663 should lead to a stabilization of the deprotonated form of Glu206 carboxylate and therefore to a more pronounced acidity of Glu206.

A lower  $pK_a$  (negative log of the acid dissociation constant  $K_a$ ) would result in a negatively charged Glu206, even in a slightly acidic environment. On the other hand, in FAP, Ala657 does not influence the acidity of Glu204. The proximity of the vicinal Glu203 and its negative charge, which in turn is stabilized by the salt bridge formed with Arg123, conversely leads to a higher  $pK_a$  of Glu204. Calculations of  $pK_a$  (Supporting Information Table S3) appeared to confirm this assumption.

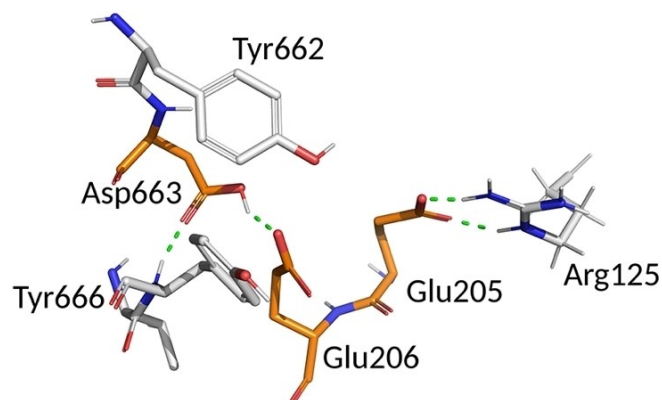


**Figure 7.** Hydrogen-bonding pattern around the Glu dyad in DPP-4. Asp663 is completely buried and protonated to interact with Glu206, while Glu205 is involved in hydrogen bonding with Arg123. DPP-4: type 4 dipeptidyl peptidase.

The conformational rigidification of the glutamate site is enforced by formation of a hydrogen bond between the protonated Asp663 side chain and the Glu206 carboxylate in DPP-4. This rigidification and the enhanced electronegative surface potential generated by the more acidic Glu206 carboxylate group act jointly to create an enhanced polar protein-ligand interaction pattern. The enhanced interaction pattern is a result of the strengthened hydrogen bonding reinforced ionic interaction between the aminopiperidine of linagliptin and Glu206.

The tighter interaction with the charged amino group of linagliptin results in a strong stabilization of the bound state and a marked reduction of the dissociation rate. Fibroblast activation protein has a lower level of stabilization of binding to the aminopiperidine moiety of linagliptin, leading to the fast binding kinetics observed at neutral pH. At basic pH, Glu204 in FAP is deprotonated, which explains the retardation of linagliptin dissociation and the increase in affinity.

The pH dependence of FAP and DPP-4 enzymatic activity presented was rationalized based on the electrostatic considerations and  $pK_a$  calculations (Supporting Information Table S3). The different  $pK_a$  values of Glu206 and Glu204 (interacting with DPP-4 and FAP, respectively) results in the presence of a permanently negatively charged Glu206, even in an acidic environment. In FAP, less acidic Glu204 is protonated at a pH range of 7 to 8. Below approximately pH 6, FAP is no longer able to bind DPP substrates productively. The influence of the protonation state of the Glu204/Glu206 residues in FAP/DPP-4 explained the observed pH dependence of wild-type FAP and the DPP-4 D663A mutant exopeptidase activities with inflection points at approximately pH 7.5, which were likely due to the Glu204/Glu206  $pK_a$  values of between 7 and 8. In contrast, since the protonation states of the Glu204/Glu206 residues are less involved in substrate recognition and catalysis for noncharged endopeptidase substrates, comparatively little change in enzyme activity of FAP and the DPP-4 D663A mutant was observed across the range of pH 6 to pH 9 (Figure 6C and 6D).

### Role of second shell amino acids in determining functional properties of proteins

We demonstrated that the distinct binding affinity and kinetics of linagliptin to FAP- $\alpha$  and DPP-4 are determined by a single amino acid difference in the vicinity of, but not directly lining, the ligand-binding sites of both proteases. The influence of Asp663 in DPP-4 and Ala657 in FAP on the affinity and kinetics of linagliptin binding to FAP- $\alpha$  and DPP-4 is in line with the role of these residues in determining enzyme activity profiles and substrate specificity.<sup>[7,14,23]</sup>

The effect of second shell residues on binding affinity and kinetics in protein-ligand interactions is poorly documented. Several groups have reported observations similar to ours.<sup>[25–28]</sup> One study described a role for the remote residue Phe46 in myoglobin on ligand binding.<sup>[25]</sup> Another highlighted the role of the second shell in protein-metal recognition.<sup>[27]</sup> Specifically, a study of zinc finger structures demonstrated the significance of

second layer packing in shielding the negatively charged zinc finger cores. Profound effects on ligand-binding modes and affinities in trypsin mutants, accounted for by differences in protein structure and dynamics, have also been shown.<sup>[28]</sup> A study investigating isoform selectivity's of antagonists for corticotropin releasing factors receptor 1 and receptor 2 showed hydrogen-bond formation in the second shell around the ligand-binding site to be a determining factor for functional selectivity.<sup>[26]</sup>

Our biophysical investigations indicated that second shell residues may have a profound and dominant effect on binding affinity and kinetics. Linagliptin dissociation from FAP was 20,000-fold faster than that for dissociation from DPP-4 at physiologic pH. In this case we showed that the introduction of a buried Asp residue affects protein dynamics and electrostatic surface potential of the binding site, leading to pronounced changes in the dissociation rates of binding ligands.

### Fibroblast activation protein inhibition by linagliptin does not support cancer therapy potential

Upregulation of FAP is notable in a wide variety of cancers, and is often used as a biomarker for protumorigenic stroma. It has also been proposed as a molecular target of cancer therapies. Much research in recent years has focused on the design and testing of diverse FAP-targeted treatments.<sup>[9]</sup> As linagliptin is the only globally approved DPP-4 inhibitor that significantly inhibits FAP- $\alpha$  in a nanomolar range, this prompted us to investigate linagliptin's potential anticancer activity through inhibition of FAP. We showed that FAP inhibition was pH dependent with a strong increase in potency as pH increased from 6 to 9. With  $IC_{50}$  89 nM at pH 7.5 and a clinical maximum plasma concentration of 12 nM at steady state using the clinically established oral dose of 5 mg,<sup>[3]</sup> clinically relevant FAP- $\alpha$  inhibition under treatment conditions will not be achieved. In addition, tumor stroma is typically characterized by an acidic environment; here, we showed that FAP- $\alpha$  inhibition by linagliptin was in the 10  $\mu$ M range, much higher than  $IC_{50}$  at neutral pH. In single rising dose studies, the highest tolerable dose of 600 mg linagliptin obtained maximal plasma concentrations in the range of 4  $\mu$ M.<sup>[29]</sup> Thus, in principle higher doses of linagliptin could generate plasma levels to inhibit FAP relevant for other indications. However, these levels are achieved only in a 120-fold higher dose than the approved 5 mg tablet, and would still not be enough to inhibit FAP sufficiently in an acidic environment of tumor stroma. These findings certainly reflect previous experience with other FAP inhibitors like PT100 (talabostat), which were investigated clinically for their potential in cancer indications. Despite demonstrating early promise in terms of the preclinical data, PT100 showed minimal efficacy in the clinical setting, even when used in combination with other chemotherapies.<sup>[30,31]</sup> The reasons for this failure are not fully understood.<sup>[9]</sup>

Type 4 dipeptidyl peptidase is the most prominent member of the S9 family, inhibition of which has led to the development of one of the most commercially and clinically successful drug

classes, the DPP-4 inhibitors.<sup>[5]</sup> In contrast, FAP, the closest homolog of DPP-4 within the family, has not been explored extensively as a therapeutic target; this oversight can be partially attributed to its relatively restrictive expression and the lack of knowledge of naturally occurring substrates. The recent discovery of FGF21 as an FAP substrate, its role in metabolic diseases,<sup>[32]</sup> and the availability of more FAP-selective compounds such as CPD60 for use in investigative studies,<sup>[17]</sup> could herald new interest in the field. In particular, potential improvement of glucose homeostasis has been investigated with CPD60 in relevant models of diabetes,<sup>[33]</sup> and a recent study demonstrated similar glucose-lowering effects with the FAP/DPP-4 unselective compound, PT100.<sup>[32,33]</sup>

Our study, which seeks to understand specific features that characterize linagliptin binding to DPP-4 and FAP, contributes to the growing body of evidence that could justify the development of optimized FAP inhibitors or biselective DPP-4/FAP inhibitors. This could lead to the development of drugs with a long-lasting duration of action for use in a greater range of metabolic disorders and their associated manifestations.

## Conclusion

The comparison of biophysical and structural mechanisms of linagliptin binding to DPP-4 and FAP indicated that second shell residues have a dominant effect on binding affinity and kinetics. We conclude that one single amino acid difference is the major determinant. We further show that the same amino acid is causal for the distinct pH-dependent activity profiles of the two DPP family members. While linagliptin does not display any anticancer activity at therapeutic doses, our findings may guide future studies for the development of optimized FAP and biselective DPP-4/FAP inhibitors.

## Experimental Section

### Materials

Linagliptin was synthesized at Boehringer Ingelheim Pharma GmbH & Co. KG, Biberach, Germany, and had a general purity of > 95 % as determined by high performance liquid chromatography and proton nuclear magnetic resonance.

### Methods

**Protein expression and purification.** Expression and purification of FAP- $\alpha$  and DPP-4 were performed according to literature protocols at Proteros Biostructures, Munich, Germany.<sup>[7]</sup> The protein was purified using Ni-NTA affinity and gel filtration chromatography steps as described in Aertgeerts et al.<sup>[14]</sup> Fibroblast activation protein- $\alpha$  A657D and DPP-4 D663A mutants were expressed and purified as FAP- $\alpha$ . This procedure yielded homogeneous proteins with a purity > 95 % as judged from Coomassie-stained SDS-PAGE.

**Enzymatic assays.** Compounds were dissolved in DMSO (final concentration 0.1 % [w/v]). Inhibition of human recombinant DPP-4 (10 ng/well), FAP- $\alpha$  (14 ng/well), DPP-4 D663A mutant (10 ng/well), or FAP A657D mutant (14 ng/well) (all from Proteros Biostructures,

Munich, Germany) activity was assayed in black 96-well plates in assay buffer (100 mM Tris, 100 mM NaCl, adjusted to the indicated pH with HCl or NaOH) in the presence of 80  $\mu$ M substrate (H-Ala-Pro-7-amido-4-trifluoromethylcoumarin [AlaPro-AFC], from Bachem) at room temperature for 1 h. Fluorescence was detected using a Wallac, Victor™ 1420 Multilabel Counter (PerkinElmer), at an excitation wavelength of 405 nm and an emission wavelength of 535 nm. A minimum of three independent experiments were used to calculate the mean values and standard deviation. For endopeptidase activity measurements, 50  $\mu$ M AC-Gly-Pro-AFC substrate was used.

**Surface plasmon resonance experiments.** Type 4 dipeptidyl peptidase and FAP were immobilized onto a CM5 chip in 10 mM sodium acetate at pH 5.5 (DPP-4) or pH 5.0 (FAP). Binding studies were performed with a Biacore T200 SPR system at 25 °C in 20 mM Tris (pH as indicated), 150 mM NaCl, 0.05 % (v/v) Tween 20, and 1 % (v/v) DMSO. Linagliptin concentrations were 0.24, 0.74, 2.2, 6.6, and 20 nM for DPP-4 binding studies, and were 15.6, 31.25, 62.5, 125, 250, and 500 nM for FAP- $\alpha$  binding studies. Binding studies for DPP-4 were performed in the single-cycle kinetic mode using 120 s association time and 7200 s dissociation time. FAP- $\alpha$  binding studies were performed in the standard kinetic program using 120 s association time and 180 s dissociation time at a flow rate of 30  $\mu$ L/min. Binding studies of the mutants were performed in the single-cycle kinetic mode using 120 s association time for the FAP A657D mutant or 180 s association time for the DPP-4 D663A mutant. Dissociation time was 7200 s for both mutants. Kinetic parameters were analyzed using the Biacore T200 Evaluation software 3.0 (GE Healthcare). At least three independent SPR experiments were used to calculate the mean values and standard deviation.

**Crystallography.** Fibroblast activation protein-alpha was combined with a molar excess of compound and concentrated to approximately 10 mg/mL. The complex was crystallized at 293 K with a reservoir solution consisting of 35 % (v/v) PEG2000MME and 0.40 M lithium salts, buffered at pH 9. Crystals were flash frozen in liquid nitrogen, and X-ray data were collected using synchrotron radiation at the X06SA beamline at the Swiss Light Source in Villigen, Switzerland (Supporting Information Table S4). Data were integrated and scaled with the XDS program package<sup>[34,35]</sup> and the structure was solved by molecular replacement with PHASER<sup>[36]</sup> using the FAP- $\alpha$  coordinates (Protein Data Bank entry 1Z68) as a search model.<sup>[7]</sup> Several rounds of building in COOT<sup>[37]</sup> and refinement with REFMAC<sup>[38]</sup> and BUSTER<sup>[39]</sup> led to the final model (detailed crystallographic data in Supporting Information Table S5). The binding pocket of FAP containing the ligand linagliptin superimposed with a 2Fo-Fc electron density map is shown in Supporting Information Figure S4. Figures 3, 4, and 7 were prepared with the PyMOL Molecular Graphics System, Version 2.0 Schrödinger, LLC.

## Acknowledgements

We are grateful to Julia Bakker and Petra Eberhardt-Härle for their excellent technical assistance. We are also grateful for medical writing assistance during the development of this manuscript which was provided by Dr Tim Hardman of Niche Science & Technology Ltd., and supported financially by Boehringer Ingelheim.

## Conflict of Interest

G.S., Y.H., R.B, T.K., and H.N. are employees of Boehringer-Ingelheim Pharma GmbH & Co. KG. P.S. is employee of Proteros Biostructures.

**Keywords:** DPP-4 · FAP · kinetics · linagliptin · pH dependence

- [1] C. Y. Edosada, C. Quan, T. Tran, V. Pham, C. Wiesmann, W. Fairbrother, B. B. Wolf, *FEBS Lett.* **2006**, *580*, 1581–1586.
- [2] C. Y. Edosada, C. Quan, C. Wiesmann, T. Tran, D. Sutherlin, M. Reynolds, J. M. Elliott, H. Raab, W. Fairbrother, B. B. Wolf, *J. Biol. Chem.* **2006**, *281*, 7437–7444.
- [3] U. Graefe-Mody, S. Retlich, C. Friedrich, *Clin. Pharmacokinet.* **2012**, *51*, 411–427.
- [4] H. U. Demuth, C. H. McIntosh, R. A. Pederson, *Biochim. Biophys. Acta.* **2005**, *1751*, 33–44.
- [5] B. Ahrén, *Front. Endocrinol.* **2019**, *10*, 376.
- [6] B. Gallwitz, *Front. Endocrinol.* **2019**, *10*, 389.
- [7] K. Aertgeerts, I. Levin, L. Shi, G. P. Snell, A. Jennings, G. S. Prasad, Y. Zhang, M. L. Kraus, S. Salakian, V. Sridhar, R. Wijnands, M. G. Tennant, *J. Biol. Chem.* **2005**, *280*, 19441–19444.
- [8] L. Juillerat-Jeanneret, P. Tafelmeyer, D. Golshayan, *Expert Opin. Ther. Targets.* **2017**, *21*, 977–991.
- [9] E. Puré, R. Blomberg, *Oncogene.* **2018**, *37*, 4343–4357.
- [10] J. E. Park, M. C. Lenter, R. N. Zimmermann, P. Garin-Chesa, L. J. Old, W. J. Rettig, *J. Biol. Chem.* **1999**, *274*, 36505–36512.
- [11] M. A. Huber, N. Kraut, J. E. Park, R. D. Schubert, W. J. Rettig, R. U. Peter, P. Garin-Chesa, *J. Invest. Dermatol.* **2003**, *120*, 182–188.
- [12] H. Staiger, M. Keuper, L. Berti, M. Hrabec de Angelis, H. U. Haring, *Endocr. Rev.* **2017**, *38*, 468–488.
- [13] A. L. Coppage, K. R. Heard, M. T. DiMare, Y. Liu, W. Wu, J. H. Lai, W. W. Bachovchin, *PLoS One.* **2016**, *11*, e0151269.
- [14] K. Aertgeerts, S. Ye, M. G. Tennant, M. L. Kraus, J. Rogers, B. C. Sang, R. J. Skene, D. R. Webb, G. S. Prasad, *Protein Sci.* **2004**, *13*, 412–421.
- [15] H. B. Rasmussen, S. Branner, F. C. Wiberg, N. Wagtmann, *Nat. Struct. Biol.* **2003**, *10*, 19–25.
- [16] M. Eckhardt, E. Langkopf, M. Mark, M. Tadayyon, L. Thomas, H. Nar, W. Pfrngle, B. Guth, R. Lotz, P. Sieger, H. Fuchs, F. Himmelsbach, *J. Med. Chem.* **2007**, *50*, 6450–6453.
- [17] K. Jansen, L. Heirbaut, R. Verkerk, J. D. Cheng, J. Joossens, P. Cos, L. Maes, A. M. Lambeir, I. De Meester, K. Augustyns, P. Van der Veken, *J. Med. Chem.* **2014**, *57*, 3053–3074.
- [18] G. Schnapp, T. Klein, Y. Hoevels, R. A. Bakker, H. Nar, *J. Med. Chem.* **2016**, *59*, 7466–7477.
- [19] S. Sun, C. F. Albright, B. H. Fish, H. J. George, B. H. Selling, G. F. Hollis, R. Wynn, *Protein Expression Purif.* **2002**, *24*, 274–281.
- [20] R. Thoma, B. Löffler, M. Stihle, W. Huber, A. Ruf, M. Hennig, *Structure.* **2003**, *11*, 947–959.
- [21] J. M. Sutton, D. E. Clark, S. J. Dunsdon, G. Fenton, A. Fillmore, N. V. Harris, C. Higgs, C. A. Hurley, S. L. Krintel, R. E. MacKenzie, A. Duttaroy, E. Gangl, W. Maniara, R. Sedrani, K. Namoto, N. Ostermann, B. Gerhartz, F. Sirockin, J. Trappe, U. Hassiepen, D. K. Baeschlin, *Bioorg. Med. Chem. Lett.* **2012**, *22*, 1464–1468.
- [22] M. Nabeno, F. Akahoshi, H. Kishida, I. Miyaguchi, Y. Tanaka, S. Ishii, T. Kadowaki, *Biochem. Biophys. Res. Commun.* **2013**, *434*, 191–196.
- [23] S. A. Meadows, C. Y. Edosada, M. Mayeda, T. Tran, C. Quan, H. Raab, C. Wiesmann, B. B. Wolf, *Biochemistry.* **2007**, *46*, 4598–4605.
- [24] A. C. Pan, D. Borhani, R. O. Dror, D. E. Shaw, *Drug Discovery Today* **2013**, *18*, 667–673.
- [25] H. H. Lai, T. Li, D. S. Lyons, G. N. Phillips Jr, J. S. Olson, Q. H. Gibson, *Proteins.* **1995**, *22*, 322–339.
- [26] X. Sun, J. Cheng, X. Wang, Y. Tang, H. Agren, Y. Tu, *Sci. Rep.* **2015**, *5*, 8066.
- [27] M. K. Tiwari, V. C. Kalia, Y. C. Kang, J. K. Lee, *Mol. Biosyst.* **2014**, *10*, 3255–3263.
- [28] A. Tziridis, D. Rauh, P. Neumann, P. Kolenko, A. Menzel, U. Brauer, C. Ursel, P. Steinmetzer, J. Sturzebecher, A. Schweinitz, T. Steinmetzer, M. T. Stubbs, *Biol. Chem.* **2014**, *395*, 891–903.
- [29] Huttner S, Graefe-Mody EU, Withopf B, Ring A, Dugi KA. Safety, tolerability, pharmacokinetics, and pharmacodynamics of single oral

- doses of BI 1356, an inhibitor of dipeptidyl peptidase 4, in healthy male volunteers. *J Clin Pharmacol.* 2008;48:1171–1178.
- [30] C. C. Cunningham, *Expert Opin. Invest. Drugs* **2007**, *16*, 1459–1465.
- [31] R. M. Eager, C. C. Cunningham, N. Senzer, D. A. Richards, R. N. Raju, B. Jones, M. Uprichard, J. Nemunaitis, *Clin. Oncol.* **2009**, *21*, 464–472.
- [32] M. A. Sánchez-Garrido, K. M. Habegger, C. Clemmensen, C. Holleman, T. D. Müller, D. Perez-Tilve, P. Li, A. S. Agrawal, B. Finan, D. J. Drucker, M. H. Tschöp, R. D. DiMarchi, A. Kharitonov, *Mol. Metab.* **2016**, *5*, 1015–1024.
- [33] B. L. Panaro, A. L. Coppage, J. L. Beaudry, E. M. Varin, K. Kaur, J. H. Lai, W. Wu, Y. Liu, W. W. Bachovchin, D. J. Drucker, *Mol. Metab.* **2019**, *19*, 65–74.
- [34] W. Kabsch, *Acta Crystallogr. Sect. D* **2010**, *66*, 125–132.
- [35] Y. Kuang, Y. Wu, H. Jiang, D. Wu, *J. Biol. Chem.* **1996**, *271*, 3975–3978.
- [36] A. J. McCoy, R. W. Grosse-Kunstleve, P. D. Adams, M. D. Winn, L. C. Storoni, R. J. Read, *J. Appl. Crystallogr.* **2007**, *40*, 658–674.
- [37] P. Emsley, B. Lohkamp, W. G. Scott, K. Cowtan, *Acta Crystallogr. Sect. D* **2010**, *66*, 486–501.
- [38] G. N. Murshudov, A. A. Vagin, E. J. Dodson, *Acta Crystallogr. Sect. D* **1997**, *53*, 240–255.
- [39] E. Blanc, P. Roversi, C. Vonrhein, C. Flensburg, S. M. Lea, G. Bricogne, *Acta Crystallogr. Sect. D* **2004**, *60*, 2210–2221.

---

Manuscript received: August 4, 2020

Revised manuscript received: September 28, 2020

Accepted manuscript online: October 8, 2020

Version of record online: October 21, 2020